Histochem Cell Biol (2012) 137:261–267
DOI 10.1007/s00418-011-0891-2

SHORT COMMUNICATION

Tangle evolution linked to differential 3- and 4-repeat tau isoform deposition: a double immunofluorolabeling study using two monoclonal antibodies

Toshiki Uchihara · Makoto Hara · Ayako Nakamura · Katsuiku Hirokawa

Accepted: 13 November 2011 / Published online: 25 November 2011

Abstract Double immunofluorolabeling for 3-repeat (3R) and 4-repeat (4R) tau was performed with two monoclonal antibodies, RD3 and RD4, after an additional pretreatment with potassium permanganate and oxalic acid to eliminate nonspecific 3R tau cytoplasmic staining. This method involves hyperdilution of one of the primary monoclonal antibodies (≥100-fold), making it undetectable by usual secondary antibodies. The hyperdiluted primary antibody can then only be detected after tyramide amplification. Subsequent application of the other monoclonal antibody at its usual concentration allows double immunofluorolabeling without cross-reaction. This novel method revealed that tau immunoreactivity (IR) in the hippocampal pyramidal neurons of Alzheimer's disease (AD) brains is heterogeneous in that pretangle neurons exhibit 4R-selective (3R−/4R+) IR, ghost tangles exhibit 3R-selective (3R+/4R−) IR, and neurofibrillary tangles exhibit both 3R and 4R (3R+/4R+) IR. Some nigral neurons exhibited RD3 IR in both AD and corticobasal degeneration/progressive supranuclear palsy (CBD/PSP) brains. However, in CBD/PSP cases, 3R IR was always superimposed on 4R IR, while 3R-selective neurons were present in AD cases. These differential isoform profiles may provide a pivotal molecular reference, closely related to the morphological evolution of tau-positive neurons, which may be variable according to disease (CBD/PSP vs. AD), lesion site (cerebral cortex and substantia nigra), or the stage of evolution (from pretangles to ghost tangles). These findings should provide a more comprehensive understanding of the histological differentiation of various tau deposits in human neurodegenerative disease.

Keywords Tau isoform · Double immunofluorolabeling · Neurofibrillary tangles · Alzheimer's disease · Corticobasal degeneration · Progressive supranuclear palsy

T. Uchihara (✉) · M. Hara · A. Nakamura
Laboratory of Structural Neuropathology,
Tokyo Metropolitan Institute of Medical Science,
2-1-6 Kamikitazawa, Setagaya, Tokyo 156-8509, Japan
e-mail: uchihara-ts@igakuken.or.jp

K. Hirokawa
Department of Pathology, Nakano General Hospital,
4-59-16 Chuo, Nakano, Tokyo 164-8607, Japan

Introduction

Tau deposits are classified biochemically according to their isoform profiles. Pick body disease is characterized by 3-repeat (3R) tau deposits (Uchihara and Tsuchiya 2008), while progressive supranuclear palsy (PSP) and corticobasal degeneration (CBD) are thought to contain predominantly 4-repeat (4R) tau deposits (Delacourte 2008; Flament et al. 1991). Although homogenates of Alzheimer's disease (AD) brains include both 3R and 4R tau, it is still unclear how differences in the expression and function of these isoforms at the cellular or subcellular level may affect tau deposition.

Despite the development of isoform-specific antibodies, RD3 and RD4 against 3R and 4R tau, respectively (de Silva et al. 2003), specific immunohistochemical differentiation of each isoform has been hampered by diffuse RD3 immunoreactivity (IR) in the neuronal cytoplasm, most likely representing normal 3R tau (de Silva et al. 2003; Hanger et al. 2002). Recently, we found that an additional pretreatment with potassium permanganate and oxalic acid, prior to the standard pretreatment with formic acid and autoclaving, successfully eliminated this diffuse RD3 IR in formalin-fixed, paraffin-embedded brain samples with tau

deposits (Uchihara et al. 2011). Precise immunolocalization of pathological 3R tau using this method demonstrated the presence of 3R tau-positive neurons in the substantia nigra (SN) in CBD/PSP, the so-called 4R tauopathies.

To observe the spatial relationship between 3R and 4R tau in more detail, double fluorolabeling to differentiate 3R and 4R tau is necessary but difficult to achieve, because the antibodies against 3R and 4R tau (RD3 and RD4, respectively) are both mouse IgG antibodies. Here, double immunofluorolabeling was accomplished by a combination of tyramide amplification of the signal from a hyperdiluted primary antibody, followed by conventional immunofluorolabeling of the other primary antibody (Hunyady et al. 1996; Nakamura and Uchihara 2004; Uchihara et al. 2000, 2003). Although both AD and PSP/CBD brains contained 3R tau-positive neurons, the SN neurons from PSP/CBD cases were characterized by the presence of 3R IR only in conjunction with 4R IR.

Materials and methods

Four patients with AD (an 87-year-old man, a 79-year-old woman, an 85-year-old man, and a 93-year-old woman), two patients with PSP (both 71-year-old men), and a patient with CBD (a 68-year-old man) were enrolled in this study. Pathological diagnoses were based on the published criteria (Dickson et al. 2002; Hauw et al. 1994; Litvan et al. 1996).

Five-micron-thick, formalin-fixed, paraffin-embedded sections from the hippocampus and the midbrain were used for immunohistochemical analysis. After deparaffinization, serial pretreatment with potassium permanganate (0.25% for 15 min), oxalic acid (2% for 3 min), formic acid (>99%, 30 min), and autoclaving (120°C in 0.05 M citrate buffer for 20 min) was performed to eliminate diffuse non-pathologic IR of RD3 (clone 8E6/C11, Upstate, Lake Placid, NY) and to enhance RD4 (clone 1E1/A6, Upstate) IR (Uchihara et al. 2011). After pretreatment with hydrogen peroxide (1%, 15 min), sections were incubated with bovine serum albumin (5%, Nacalai, Kyoto, Japan) diluted in phosphate-buffered saline containing 0.03% Triton X 100 (PBST, Wako, Tokyo, Japan).

To perform double immunofluorolabeling with two antibodies of the same class from the same species (mouse monoclonal IgG), one of the antibodies was serially hyperdiluted to find the antibody concentration at which the target epitope is immunofluorolabeled after amplification with biotinylated tyramide but not without amplification. To determine this concentration, different dilutions of one of the antibodies were also probed in parallel with an anti-mouse IgG conjugated with horseradish peroxidase (1:200), amplified with biotinylated tyramide (1:1,000, Perkin Elmer), and visualized with streptavidin-Alexa 488 Fluor® (1:200, Molecular Probe, Carlsbad, CA, USA). After this amplified-immunofluorolabeling, the other antibody was applied at its usual concentration (1:300 for RD3 and 1:100 for RD4). Because the secondary anti-mouse antibody conjugated with Alexa Fluor® 546 (1:200, Molecular Probe) is not sensitive enough to label the hyperdiluted antibody of the first cycle, it selectively labels the primary antibody of the second cycle without cross-reacting with the hyperdiluted antibody (Hunyady et al. 1996; Uchihara et al. 2003).

Double-labeled sections were mounted with glycerol containing *p*-phenylenediamine and observed under a confocal microscope (Leica SP5, Heidelberg, Germany) equipped with multiple laser lines. Midbrain sections were scanned for their fluorescent profiles with high-resolution digital micrographs (0.33 μm/pixel, with 20× objective) that overlapped each other and were automatically tiled to encompass the entire 2D area of the preparation. Tiled two-dimensional double-fluorescent images (maximum 26 × 64 mm^2 area) were screened to identify tau-positive lesions in the SN (VS120, Olympus, Tokyo, Japan) (Kanazawa et al. in press). After identifying representative regions of interest, detailed images were obtained using confocal microscopy.

Results

Although not detectable using the usual secondary antibody (anti-mouse IgG) conjugated with Alexa 488 Fluor® (Fig. 1b), it was possible to visualize the RD3 antibody after its hyperdilution (1:30,000) through amplification with biotinylated tyramide (Figs. 1a, 2c, green). Subsequent RD4 immunostaining at the usual concentration (1:100) was labeled by a secondary antibody conjugated with Alexa Fluor® 546 (Fig. 2b, red). Because this secondary antibody is not sensitive enough to label the hyperdiluted primary antibody (Fig. 1b) of the first cycle, it selectively labeled RD4 without cross-reacting with RD3. As a result, double labeling with tyramide-amplified RD3 (1:30,000, Fig. 2c, green) and non-amplified RD4 (1:100, Fig. 2b, red) was possible even though RD3 and RD4 are both mouse-monoclonal antibodies (Fig. 2a, merged). Double labeling with tyramide-amplified hyperdiluted RD4 (1:10,000, Fig. 2e, green) followed by non-amplified RD3 (1:300, Fig. 2f, red) yielded an essentially identical picture with reversal of the color representation (Fig. 2a, d) on neighboring sections of the hippocampus.

Tau-positive neurons were either 4R selective (3R−/4R+, green empty arrowhead, Fig. 2g–i), 3R selective (3R+/4R−, Fig. 2g–i, red empty arrowhead), or both 3R and 4R positive (3R+/4R+, Fig. 2g–i, yellow empty

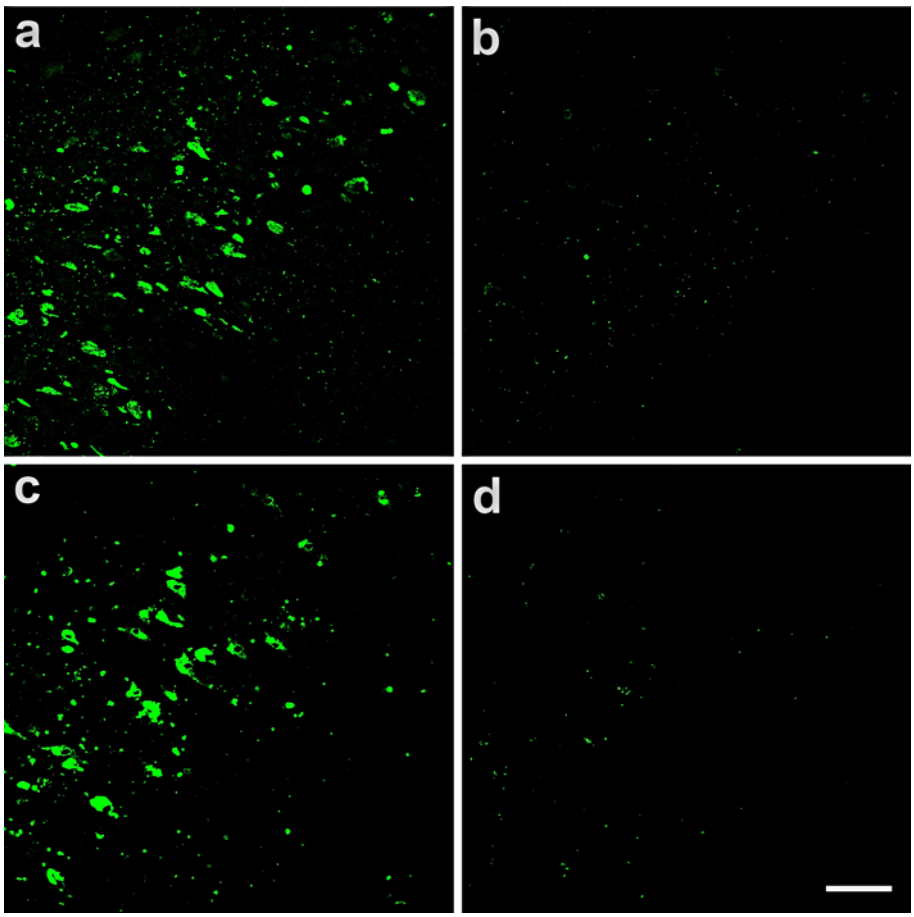

Fig. 1 Enhanced fluorescent signal by biotinylated tyramide. Hyperdiluted primary antibodies (RD3, 1:30,000 for **a, b** and RD4, 1:10,000 for **c, d**) are detectable after signal enhancement with biotinylated tyramide (**a, c**) but not with conventional secondary antibodies (**b, d**). Hippocampal pyramidal neurons from a patient with Alzheimer disease (AD). Bar = 100 μm

arrowhead). These immunohistochemical tau isoform profiles largely correlated with different morphological characteristics of tau-positive neurons. For example, pretangle neurons without apparent fibrillary structure were 4R selective (3R−/4R+, green), while ghost tangles with loosened coarse fibrils were 3R selective (3R+/4R−, red). Typical neurofibrillary tangles with compact fibrillary structures were both 3R and 4R positive (NFTs, 3R+/4R+, yellow). Scanning the entire midbrain for these fluorescent profiles was very helpful in finding the appropriate regions of interest (ROIs) in the SN (Fig. 3a, b). In AD brains (Fig. 3a, c, e), neurons in both the hippocampus and the SN were either 3R−/4R+ (green), 3R+/4R+ (yellow), or 3R+/4R− (red). This is in contrast with CBD cases (Fig. 3b, d, f), where 3R+/4R− (red) neurons were absent, and 3R IR was always superimposed on 4R IR in the SN (Fig. 3f). A similar profile was observed in the SN of PSP brains.

Discussion

Tau isoform-specific immunostaining became feasible after introduction of the monoclonal antibodies RD3 and RD4, which distinguish 3R and 4R tau, respectively (de Silva et al. 2003). Unfortunately, immunostaining with the RD3 antibody sometimes results in diffuse cytoplasmic staining, thereby complicating the differentiation between 3R and 4R tau in formalin-fixed, paraffin-embedded samples (de Silva et al. 2003). Recently, we were successful in eliminating this diffuse cytoplasmic staining, most likely representing normal 3R tau, by additional pretreatment with potassium permanganate and oxalic acid prior to conventional formic acid, and autoclaving. Moreover, this pretreatment was found to enhance RD4 IR (Uchihara et al. 2011), suggesting that the RD4 epitope is conformationally modified by the additional pretreatment (Espinoza et al. 2008).

Here, we have capitalized on the improved RD4 IR and selective pathological 3R tau immunostaining obtained using our additional pretreatment to achieve double immunofluorolabeling using these two mouse monoclonal antibodies. Cross-reaction between the two mouse-antibodies was successfully avoided by hyperdiluting one of the primary antibodies (1:30,000 for RD3 and 1:10,000 for RD4). After hyperdilution, the usual secondary antibody failed to label this primary antibody, and the signal could only be visualized after amplification with biotinylated tyramide. Based on this difference in the detection thresholds, the first cycle was performed with the

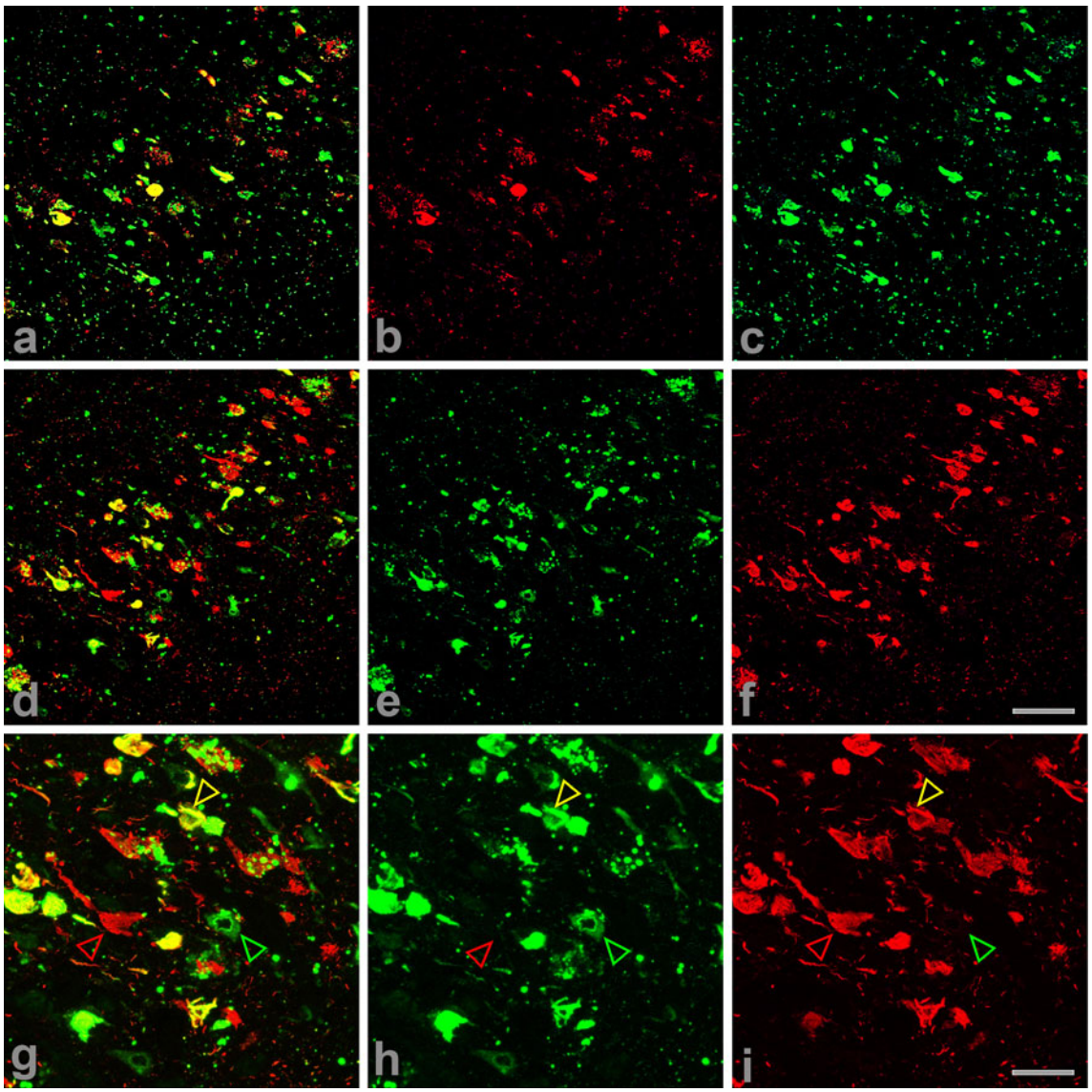

Fig. 2 Double immunofluorolabeling with two monoclonal antibodies RD3 and RD4, specific to three repeat (3R) and four repeat (4R) tau. Hippocampal pyramidal neurons of AD patient. In the first cycle, one of the monoclonal antibodies (RD3, 1:30,000 for **c** or RD4, 1:10,000 for **e, h**) was hyperdiluted and tyramide-amplified to be visualized with Alexa488 (*green*). The second cycle labeling with the other antibody at usual dilution (RD3, 1:300 for **f, i**, or RD4, 1:100 for **b**) was labeled with an anti-mouse IgG conjugated with Alexa 546 (*red*). This anti-mouse IgG conjugated with Alexa 546 (*red*) selectively labels the primary antibody at usual dilution in the second cycle, because it is not sensitive enough to label the hyperdiluted antibody in the first cycle. 3R-selective neurons (3R+/4R−: *red empty arrowheads*, **g–i**) consist of coarse fibrillary structures, resembling ghost tangles. In contrast, 4R-selective neurons (3R−/4R+: *green empty arrowheads*, **g–i**) lack fibrillary structure, resembling pretangle neurons. Neurons positive for both 3R and 4R (3R+/4R+: *yellow empty arrowheads*, **g–i**) are typical neurofibrillary tangles. **b, e, h**: 4R tau, **c, f, i**: 3R tau, **a, d, g**: *merged*. Bar = 100 μm: **a–f**. Bar = 50 μm: **g–i**

hyperdiluted antibody to be detected after amplification. It was then possible to apply the other primary antibody at its usual concentration (1:300 for RD3 and 1:100 for RD4) to be detected selectively with a conventional secondary antibody without cross-reaction to the hyperdiluted antibody of the first cycle (Hunyady et al. 1996; Nakamura and Uchihara 2004; Uchihara et al. 2003). Comparison of neighboring sections in which RD3 or RD4 was amplified (Fig. 2a–f) confirmed that each antibody exhibits essentially the same isoform profile not influenced by tyramide amplification. This established that the double labeling was sensitive and well balanced enough to display both RD3 and RD4 epitopes in equivalent intensities (Fig. 2a–f).

In agreement with previously published results, both 3R and 4R tau IR were present in hippocampal neurons from AD brains; however, isoform profiles were highly heterogeneous from one neuron to another. Immunostaining was either 4R-selective (3R−/4R+, Fig. 2g–i, green empty

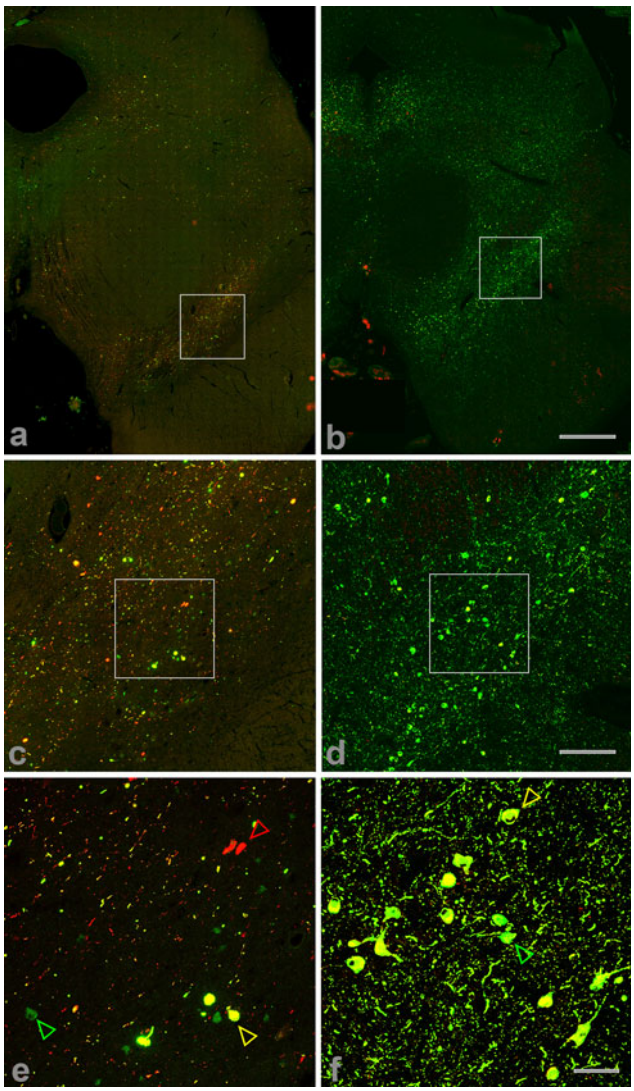

Fig. 3 Double immunofluorolabeling for 3R (*red*) and 4R (*green*) tau in the midbrain of AD and corticobasal degeneration (CBD). Double labeled midbrain sections were scanned for their fluorescent profile with high resolution digital micrographs to encompass the entire midbrain area (**a, b**, see "Materials and methods" for details). Progressive close up views of the *squares* in **a, c** for AD and those in **b, d** for CBD. 4R-selective neurons (3R−/4R+: *green empty arrownead*) and neurons positive for both 3R and 4R (3R+/4R+: *yellow empty arrowhead*) are present in the substantia nigra of AD and CBD brains. 3R-selective neurons, present in AD (3R+/4R−: *red empty arrowhead* **e**), are absent in CBD (**f**). Bar = 1 mm: **a, b**. Bar = 500 μm: **c, d**. Bar = 100 μm: **e, f**

arrowhead), 3R-selective (3R+/4R−, Fig. 2g–i, red empty arrowhead) or positive for both 3R and 4R (3R+/4R+, Fig. 2g–i, yellow empty arrowhead). Furthermore, differences in tau isoform profiles correlated with distinctive morphologies of tau-positive neurons. Namely, 4R-selective (3R−/4R+, Fig. 2, green) neurons exhibited diffuse cytoplasmic IR without apparent fibrillary structures, resembling the so-called "pretangle neurons" (Bancher et al. 1989; Iseki et al. 2001; Jellinger and Attems 2007; Uchihara et al. 2001). In contrast, most of the 3R-selective (3R+/4R−, Fig. 2, red) neurons were characterized by loosened, widely spaced parallel fibers, compatible with ghost tangles. Neurons positive for both 3R and 4R tau largely correlated with typical NFTs with tight fibrillary structures.

These findings are compatible with previous observations that pretangle neurons are positive for 4R tau and ghost tangles are positive for 3R tau (Espinoza et al. 2008; Iseki et al. 2006; Jellinger and Attems 2007; Kitamura et al. 2005; Lace et al. 2009). However, this correlation may be debatable if the diffuse cytoplasmic staining of RD3 noted previously (de Silva et al. 2003) actually represents the non-fibrillary tau deposits found in pretangles. The combined pretreatment with potassium permanganate and oxalic acid established in our earlier study provides clarity by eliminating the diffuse RD3 staining and selectively labeling the apparent fibrillary structure of NFTs (Uchihara et al. 2011). In addition, double immunofluorolabeling with RD3 and RD4 antibodies clearly demonstrates the difference between pretangles that are 4R-selective (3R−/4R+, green) and ghost tangles that are 3R-selective (3R+/4R−, red), which has not been achieved in previous single-labeling studies or double-labeling studies without this combination of pretreatments.

Cortical neurons in CBD/PSP are usually 4R-selective, while some of their brainstem neurons exhibit RD3 IR, similar to neurons in AD brains (Uchihara et al. 2011; Yoshida 2006). However, double labeling with RD3 and RD4 antibodies demonstrated for the first time that in nigral neurons of CBD/PSP, RD3 IR is always superimposed on RD4-positive neurons (Fig. 3f). In other words, 3R-selective neurons (3R+/4R−, Fig. 3e, red empty arrowhead) are absent in the SN of CBD/PSP (Fig. 3b, d, f), but present in AD brains, not only in the hippocampus and cortex but also in the SN (Fig. 3e). This is the first demonstration that 3R-selective neurons found in AD are absent in CBD/PSP.

Chronological evolution from 4R-selective pretangle neurons to 3R- and 4R-positive neurofibrillary tangles and then to 3R-selective ghost tangles (Jellinger and Attems 2007; Lace et al. 2009) in AD may be shared with CBD/PSP. Indeed, abundant pretangle neurons in the extrahippocampal cortex of CBD/PSP (Li et al. 1998) may be related to their 4R-selective profile (Uchihara et al. 2011), possibly representing an earlier phase of tau deposition. This is in contrast with the more frequent 3R+/4R+ neurons and rare pretangles in AD neocortex (Iseki et al. 2006; Jellinger and Attems 2007; Li et al. 1998), representing an advanced phase of tau deposition. Additional 3R IR superimposed on 4R IR in nigral neurons present in CBD/PSP may also represent an

advanced stage of tau deposition. In this context, the lack of 3R-selective neurons in CBD/PSP may be correlated with the relative lack of ghost tangles in CBD/PSP compared with AD (Arima et al. 1999; Jin et al. 2006).

It remains to be clarified how each tau isoform contributes to aggregation (Adams et al. 2010); however, recent biochemical experiments with synthetic tau have demonstrated isoform-dependent conformation of aggregates (Siddiqua and Margittai 2010), which may correspond to pathological states specific to disease. Moreover, preformed seeds may dictate a seeding barrier or trigger subsequent aggregation, where the seeding efficacy is dependent on both the isoform and conformation of the seeds and the recruited tau (Dinkel et al. 2011; Nonaka et al. 2010). For example, preformed seeds of 3R tau recruit both 3R and 4R tau, while preformed seeds of 4R tau selectively recruit 4R tau, but not 3R tau for their fibril elongation (Dinkel et al. 2011). Inability of 4R tau aggregates to recruit 3R tau may be related to the pretangle state, which is more predominant in cortical neurons of CBD/PSP. Once 3R tau is recruited, the aggregates may further recruit 3R tau to develop NFTs positive for both 3R and 4R tau. Although the underlying molecular mechanisms driving this chronological evolution remain to be identified, differential tau isoform profiles may provide a pivotal molecular reference for the morphological evolution of tau-positive neurons. This morphological evolution of tau-positive neurons is differentially represented according to disease (CBD/PSP vs. AD), lesion sites (cortex vs. brainstem), and evolution of tau deposition (pretangle to ghost tangle), and thus, potentially useful for histological differential diagnosis. Furthermore, this molecular reference may be helpful in identifying factors involved in the evolution of tau-positive deposits, which may be highly variable between diseases or even between neurons.

Conclusions

Double immunofluorolabeling using two monoclonal antibodies against 3R and 4R tau demonstrated cell-to-cell heterogeneity in their immunohistochemical profiles in tau-positive neurons in AD and CBD/PSP brains. In AD, 3R−/4+ pretangle neurons may evolve into 3R+/4R+ NFTs and finally 3R+/4R− ghost tangles, while 3R+ neurons in CBD/PSP brainstems always accompany 4R IR. Cell-to-cell discrimination of this immunohistochemical profile should provide insight into how tau proteins are differentially expressed and deposited according to different stages and in different diseases.

References

Adams SJ, DeTure MA, McBride M, Dickson DW, Petrucelli L (2010) Three repeat isoforms of tau inhibit assembly of four repeat tau filaments. PLoS One 5:e10810

Arima K, Nakamura M, Sunohara N, Nishio T, Ogawa M, Hirai S, Kawai M, Ikeda K (1999) Immunohistochemical and ultrastructural characterization of neuritic clusters around ghost tangles in the hippocampal formation in progressive supranuclear palsy brains. Acta Neuropathol 97:565–576

Bancher C, Brunner C, Lassmann H, Budka H, Jellinger K, Wiche G, Seitelberger F, Grundke-Iqbal I, Iqbal K, Wisniewski HM (1989) Accumulation of abnormally phosphorylated tau precedes the formation of neurofibrillary tangles in Alzheimer's disease. Brain Res 477:90–99

de Silva R, Lashley T, Gibb G, Hanger D, Hope A, Reid A, Bandopadhyay R, Utton M, Strand C, Jowett T, Khan N, Anderton B, Wood N, Holton J, Revesz T, Lees A (2003) Pathological inclusion bodies in tauopathies contain distinct complements of tau with three or four microtubule-binding repeat domains as demonstrated by new specific monoclonal antibodies. Neuropathol Appl Neurobiol 29:288–302

Delacourte A (2008) Tau, a biological marker of neurodegenerative diseases. In: Duyckaerts C, Litvan E (eds) Handbook of clinical neurology, vol 89 (dementias), chapter 15. Elsevier, Amsterdam, pp 161–172

Dickson DW, Bergeron C, Chin SS, Duyckaerts C, Horoupian D, Ikeda K, Jellinger K, Lantos PL, Lippa CF, Mirra SS, Tabaton M, Vonsattel JP, Wakabayashi K, Litvan I (2002) Office of Rare Diseases neuropathologic criteria for corticobasal degeneration. J Neuropathol Exp Neurol 61:935–946

Dinkel PD, Siddiqua A, Huynh H, Shah M, Margittai M (2011) Variations in filament conformation dictate seeding barrier between three- and four-repeat tau. Biochemistry 50:4330–4336

Espinoza M, de Silva R, Dickson DW, Davies P (2008) Differential incorporation of tau isoforms in Alzheimer's disease. J Alzheimers Dis 14:1–16

Flament S, Delacourte A, Verny M, Hauw JJ, Javoy-Agid F (1991) Abnormal Tau proteins in progressive supranuclear palsy: similarities and differences with the neurofibrillary degeneration of the Alzheimer type. Acta Neuropathol 81:591–596

Hanger DP, Gibb GM, de Silva R, Boutajangout A, Brion JP, Revesz T, Lees AJ, Anderton BH (2002) The complex relationship between soluble and insoluble tau in tauopathies revealed by efficient dephosphorylation and specific antibodies. FEBS Lett 531:538–542

Hauw JJ, Daniel SE, Dickson D, Horoupian DS, Jellinger K, Lantos PL, McKee A, Tabaton M, Litvan I (1994) Preliminary NINDS neuropathologic criteria for Steele–Richardson–Olszewski syndrome (progressive supranuclear palsy). Neurology 44:2015–2019

Hunyady B, Krempels K, Harta G, Mezey E (1996) Immunohistochemical signal amplification by catalyzed reporter deposition and its application in double immunostaining. J Histochem Cytochem 44:1353–1362

Iseki E, Matsumura T, Marui W, Hino H, Odawara T, Sugiyama N, Suzuki K, Sawada H, Arai T, Kosaka K (2001) Familial frontotemporal dementia and parkinsonism with a novel N296H mutation in exon 10 of the tau gene and a widespread tau accumulation in the glial cells. Acta Neuropathol 102:285–292

Iseki E, Yamamoto R, Murayama N, Minegishi M, Togo T, Katsuse O, Kosaka K, Akiyama H, Tsuchiya K, de Silva R, Andrew L, Arai H (2006) Immunohistochemical investigation of neurofibrillary tangles and their tau isoforms in brains of limbic neurofibrillary tangle dementia. Neurosci Lett 405:29–33

Jellinger KA, Attems J (2007) Neurofibrillary tangle-predominant dementia: comparison with classical Alzheimer disease. Acta Neuropathol 113:107–117

Jin C, Katayama S, Hiji M, Watanabe C, Noda K, Nakamura S, Matsumoto M (2006) Relationship between neuronal loss and tangle formation in neurons and oligodendroglia in progressive supranuclear palsy. Neuropathology 26:50–56

Kanazawa T, Adachi E, Orimo S, Nakamura A, Mizusawa H, Uchihara T (in press) Pale neurites, premature alpha-synuclein aggregates with centripetal extension from axon collaterals. Brain Pathol doi:10.1111/j.1750-3639.2011.00509.x

Kitamura T, Sugimori K, Sudo S, Kobayashi K (2005) Relationship between microtubule-binding repeats and morphology of neurofibrillary tangle in Alzheimer's disease. Acta Neurol Scandinav 112:327–334

Lace G, Savva GM, Forster G, de Silva R, Brayne C, Matthews FE, Barclay JJ, Dakin L, Ince PG, Wharton SB (2009) Hippocampal tau pathology is related to neuroanatomical connections: an ageing population-based study. Brain 132:1324–1334

Li F, Iseki E, Odawara T, Kosaka K, Yagishita S, Amano N (1998) Regional quantitative analysis of tau-positive neurons in progressive supranuclear palsy: comparison with Alzheimer's disease. J Neurol Sci 159:73–81

Litvan I, Hauw JJ, Bartko JJ, Lantos PL, Daniel SE, Horoupian DS, McKee A, Dickson D, Bancher C, Tabaton M, Jellinger K, Anderson DW (1996) Validity and reliability of the preliminary NINDS neuropathologic criteria for progressive supranuclear palsy and related disorders. J Neuropathol Exp Neurol 55:97–105

Nakamura A, Uchihara T (2004) Dual enhancement of triple immunofluorescence using two antibodies from the same species. J Neurosci Methods 135:67–70

Nonaka T, Watanabe ST, Iwatsubo T, Hasegawa M (2010) Seeded aggregation and toxicity of α-synuclein and tau: cellular models of neurodegenerative diseases. J Biol Chem 285:34885–34898

Siddiqua A, Margittai M (2010) Three- and four-repeat Tau coassemble into heterogeneous filaments: an implication for Alzheimer disease. J Biol Chem 285:37920–37926

Uchihara T, Tsuchiya K (2008) Neuropathology of Pick body disease. In: Duyckaerts C, Litvan E (eds) Handbook of clinical neurology, vol 89 (dementias), chapter 15. Elsevier, Amsterdam, pp 415–430

Uchihara T, Nakamura A, Nagaoka U, Yamazaki M, Mori O (2000) Dual enhancement of double immunofluorescent signals by CARD: participation of ubiquitin during formation of neurofibrillary tangles. Histochem Cell Biol 114:447–451

Uchihara T, Nakamura A, Yamazaki M, Mori O (2001) Evolution from pretangle neurons to neurofibrillary tangles monitored by thiazin red combined with Gallyas method and double immunofluorescence. Acta Neuropathol 101:535–539

Uchihara T, Nakamura A, Nakayama H, Arima K, Ishizuka N, Mori H, Mizushima S (2003) Triple immunofluorolabeling with two rabbit polyclonal antibodies and a mouse monoclonal antibody allowing three-dimensional analysis of cotton wool plaques in Alzheimer disease. J Histochem Cytochem 51:1201–1206

Uchihara T, Nakamura A, Shibuya K, Yagishita S (2011) Specific detection of pathological three-repeat tau after pretreatment with potassium permanganate and oxalic acid in PSP/CBD brains. Brain Pathol 21:180–188

Yoshida M (2006) Cellular tau pathology and immunohistochemical study of tau isoforms in sporadic tauopathies. Neuropathology 26:457–470